Int. J. Electrochem. Sci., 16 **(2021)** Article ID: 210834, doi: 10.20964/2021.08.02

International Journal of
ELECTROCHEMICAL
SCIENCE
www.electrochemsci.org

Square-Wave Potential-Modified Pt Particles for Methanol and Ammonia Oxidation

Wenjie Fu[1], Bin Liu[1], Jie Liu[1], Xiaopeng Han[1,2], Yida Deng[1,2], Cheng Zhong[1,2,3,] and Wenbin Hu[1,2,3]*

[1] Key Laboratory of Advanced Ceramics and Machining Technology (Ministry of Education), School of Materials Science and Engineering, Tianjin University, Tianjin 300072, China.
[2] Tianjin Key Laboratory of Composite and Functional Materials, School of Materials Science and Engineering, Tianjin University, Tianjin 300072, China.
[3] Joint School of National University of Singapore and Tianjin University, International Campus of Tianjin University, Binhai New City, Fuzhou 350207, China.
[*]E-mail: cheng.zhong@tju.edu.cn

Received: 16 April 2021 / *Accepted:* 22 May 2021 / *Published:* 30 June 2021

Platinum (Pt) particle electrocatalysts prepared by electrolytic deposition and periodic square-wave potential (PSWP) modification provide a promising alternative catalyst for the oxidation of ammonia and methanol. The whole electrochemical process avoided use the capping agent to ensure the high purity of the Pt catalyst. Dendritic and cube-like Pt particles were prepared in this work and the influences of the PSWP parameters (frequency (*f*), time (*t*), upper potential (E_U), lower potential (E_L)) on the morphologies of the Pt particles were investigated. Based on the experimental results, a lower *f* and a longer *t* lead to the dendritic morphology of the Pt particles. A higher E_U and a lower E_L are more likely to convert the Pt particles to a cube-like morphology. Interestingly, the modified Pt electrocatalyst with dendritic shape showed excellent electrocatalytic performance when performed on methanol and ammonia. Moreover, the mass-specific activity (MA) of dendritic Pt particles (Pts–Den) catalysis of methanol is approximately five times higher than that of the electrocatalysts before modification. This result can be explained by the large electrochemically active surface area (ECSA) and high electrocatalytic activity per unit area.

Keywords: Pt particles, methanol and ammonia oxidation, electrocatalysis, periodic square-wave potential

1. INTRODUCTION

Pt has been considered one of the most effective electrocatalysts for many electrochemical reactions, e.g., electrooxidation of methanol[1,2], electrooxidation of ammonia[3,4], electrooxidation of hydrazine[5], electrooxidation of ethanol[4], and oxygen reduction[6]. These electrochemical reactions

play a significant role in a wide variety of applications, such as fuel cells[7], hydrogen production[8,9] and the treatment of pollutants[10]. However, the high prices and low reserves of Pt greatly hinder its extensive commercial applications. Therefore, reducing the Pt content in electrocatalysts without negatively affecting the electrocatalytic performance has become the central issue in the development of electrocatalysts.

Previous studies have reported that the catalytic performance of electrocatalysts is strongly dependent on their morphology and structure[11-13]. Pt electrocatalysts with unique morphologies exhibit a higher specific surface area and more exposed active sites, which are advantageous for improving the electrocatalytic performance. Therefore, many Pt particles with different morphologies have been synthesized. For example, Kim and coworkers prepared Pt nanowires by treating electrospun polyvinyl pyrrolidone (PVP)-Pt composite fibers at high temperatures in an air atmosphere[14]. Ahmadi and coworkers prepared cubic Pt particles by controlling the concentration of sodium polyacrylate in the solution[15]. In addition, Yang and coworkers reduced K_2PtCl_4 with L-ascorbic acid in an aqueous solution to deposit Pt particles with a flower-like morphology on the surface of poly (sodium 4-styrenesuifonate) wrapped carbon nanotubes (PSS-CNTs)[16]. These commonly-used chemical preparation methods generally require organic additives such as surfactants, capping agents, and/or templates to prepare catalysts with different morphologies. However, the addition of these additives may introduce heterogeneous impurities, and complex post-processing is required to remove them; this post-processing may affect the morphology and structure of the electrocatalyst. Moreover, the prepared Pt particles must be transferred to the surface of the current collector to form a catalytic electrode, but the transfer may cause aggregation of the electrocatalyst and hinder its catalytic performance. In contrast, electrochemical deposition can directly grow Pt electrocatalysts on the surface of conductive substrates without using organic additives. As a result, the removal of extraneous additives and the transfer of catalysts could be avoided, which would be beneficial to the catalytic activity of the electrocatalyst. In addition, electrochemical deposition has the advantages of low cost, fast deposition rate and an easy-to-operate procedure, which provides broad prospects for large-scale production in industrial fields[17]. Compared with conventionally used electrochemical deposition methods such as galvanostatic and potentiostatic electrochemical deposition, the parameters in periodic square-wave potential (PSWP) treatment are more varied and more controllable[18], and they provide more possibilities for the preparation of Pt electrocatalysts with special morphologies. For example, Zinola and coworkers reported that the morphology of prepared Pt particles could be modified via PSWP treatment, thereby improving the catalytic activity of Pt particles[19]. However, the functional mechanisms of PSWP parameters, including upper potential (E_U), lower potential (E_L), modification time (t), and frequency (f), on the morphology and structure of Pt electrocatalysts remain unclear.

In this work, we used a two-step electrochemical method to obtain Pt particles. Smooth spherical Pt particles with a size of approximately 400–600 nm were first prepared on carbon paper by galvanostatic electrochemical deposition, and then the spherical Pt particles were modified by PSWP in a 1 M H_2SO_4 solution to obtain a series of particles with different morphologies (dendritic, cube-like, hollow). To obtain Pt particles with special morphologies that offer high performance and durability, this work studied the influence of different PSWP parameters (E_U, E_L, t, and f) on the morphology and structure of Pt particles, and the morphology evolution mechanism was further discussed. In terms of

the electrocatalytic performance during the electrochemical oxidation of methanol and ammonia, the activity of Pt particles modified by PSWP shows a significant improvement. The current density of the dendritic Pt particles when electrochemically oxidizing methanol was almost four times higher than that of the smooth spherical Pt particles. Compared with the one-step electrochemical deposition method, the PSWP-based two-step synthesis shows better potential in improving the specific activity of Pt electrocatalysts. This research demonstrates the possibility of further expanding the commercial application of Pt.

2. EXPERIMENTAL

2.1. Reagents and materials

H_2PtCl_6 was purchased from Sigma-Aldrich, and carbon paper was purchased from Toray (TGP-H-060). Concentrated H_2SO_4 was purchased from Tianjin Jiangtian Chemical Technology Co., Ltd., Tianjin, China. KOH, ammonia, and CH_3OH were purchased from Sinopharm Chemical Reagent Co., Ltd. All chemical reagents were of analytical grade and used as received. All solutions were prepared using ultrapure water (18.2 MΩ cm) obtained from a Milli-Q water purification system and deaerated by purging with high-purity argon gas (99.999%) throughout the test.

2.2. Electrochemical deposition of Pt particles

The carbon paper was cleaned in a Plamsa Cleaner (PDC-002-HP) for 20 min before the experiment, and the working gas was argon. Pt particles were deposited on a piece of carbon paper substrate in a mixed solution of 5 mM H_2PtCl_6 and 0.5 M H_2SO_4 with a constant current of –0.4 mA cm^{-2} for 2300 s. The electrochemical deposition was performed on an electrochemical workstation (CHI660E) and used a typical three-electrode system. The working electrode was a piece of carbon paper with an effective area of 1 cm^2 in contact with the electrolyte. A mercury sulfate electrode (MSE) and a Pt plate were used as the reference and counter electrodes, respectively.

2.3. Pt particles for pulse modification in the PSWP experiments

A schematic diagram of periodic square wave potential modification is shown in Figure 1. The pulse modification was implemented in the CV-INT mode of a Bipolar DC Power Supply BP4610 with a two-electrode system in 1 M H_2SO_4 solution. Carbon paper deposited with Pt particles and a carbon rod were used as the working electrode and the reference electrode, respectively. The dendritic morphology was obtained with E_U and E_L to be 0.9 V and –2.7 V, respectively. The *f* and the *t* were 10 Hz and 90 min, respectively. To obtain a cubic morphology, the E_U and E_L were adjusted to 1.0 V and –3.2 V, respectively, and *f* and *t* were 10 Hz and 35 min, respectively.

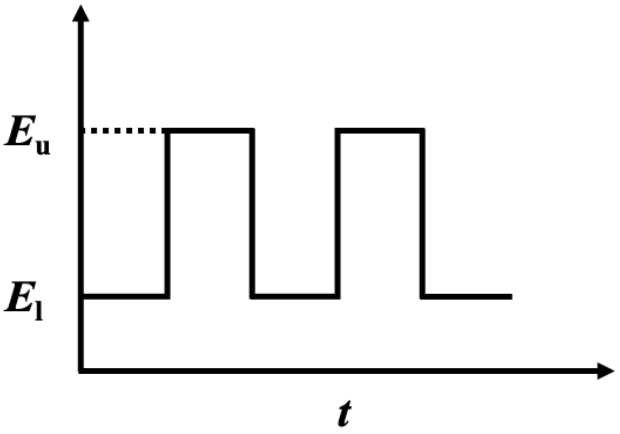

Figure 1. Schematic diagram of the periodic square wave potential modification.

2.4. Characterization of Pt loading and morphology

Thermal field-emission scanning electron microscopy (SEM, JSM-7800F) was used to observe the quantity density and surface morphology of the Pt particles, and the high-resolution morphology and structure of the Pt particles were measured by transmission electron microscopy (TEM, JEM-2100F). The exact Pt content was determined by inductively coupled plasma mass spectrometry ICPMS (NexlON 300X).

2.5. Electrochemical test

The electrochemical tests were performed on an electrochemical workstation (CHI660E). The electrocatalytic oxidation of methanol was carried out in a classic mixed solution of 0.5 M H_2SO_4 and 1 M CH_3OH at a scan rate of 0.05 V s^{-1} from 0 to 1 V (vs. SCE). The electrocatalytic activity of methanol was determined in a mixed solution of 1 M KOH and 0.1 M ammonia at a scan rate of 0.01 V s^{-1} from –1 to 0 V (vs. SCE). A typical three-electrode system was used throughout the whole process. Carbon paper with deposited Pt electrocatalyst was used as the working electrode. A Pt sheet and saturated calomel electrode (SCE) were used as the counter electrode and the reference electrode, respectively. The electrochemical surface area (ECSA) was determined by measuring the area under the hydrogen desorption peak (0.05 V s^{-1}) of the CV in 0.5 M H_2SO_4 solution. All experiments were conducted at a controlled temperature of 25±1 °C.

3. RESULTS AND DISCUSSION

Figure 2a and b show typical SEM images of the surface morphology of Pt particles electrodeposited on the carbon paper substrate. The distribution of Pt particles was dense and uniform (Figure 2a). Based on the high-magnification SEM image shown in Figure 2b, the Pt particles obtained by electrochemical deposition were all spherical Pt particles with an average diameter of approximately

400 nm–600 nm (Pts–Sph). Close examination reveals that there were slight bumps on its surface (Figure 1b).

Our previous work found that the current density and time of electrochemical deposition have a profound impact on the reduction and diffusion process of Pt ions, affecting the surface morphology of Pt deposits[20]. Therefore, electrode materials with uniform morphology and particle size were obtained by adjusting the deposition current density and deposition time, which was a basis for further study of the intrinsic relationship between the PSWP parameters and the morphology and structure of the Pt particles. The chronoamperograms response during the galvanostatic electrochemical deposition of Pt is shown in Figure 1c. The sudden drop in the initial potential could be caused by the nucleation process; then, the potential stabilized at –0.1 V(vs. MSE), which indicates the steady growth of Pt particles[21]. At a relatively low current density (−0.4 mA cm^{-2}), the slow nucleation rate provides the condition for the precursor ions to diffuse from the overall precursor solution to the surface of the substrate to uniformly grow under this deposition condition to form a quasi-spherical structure.

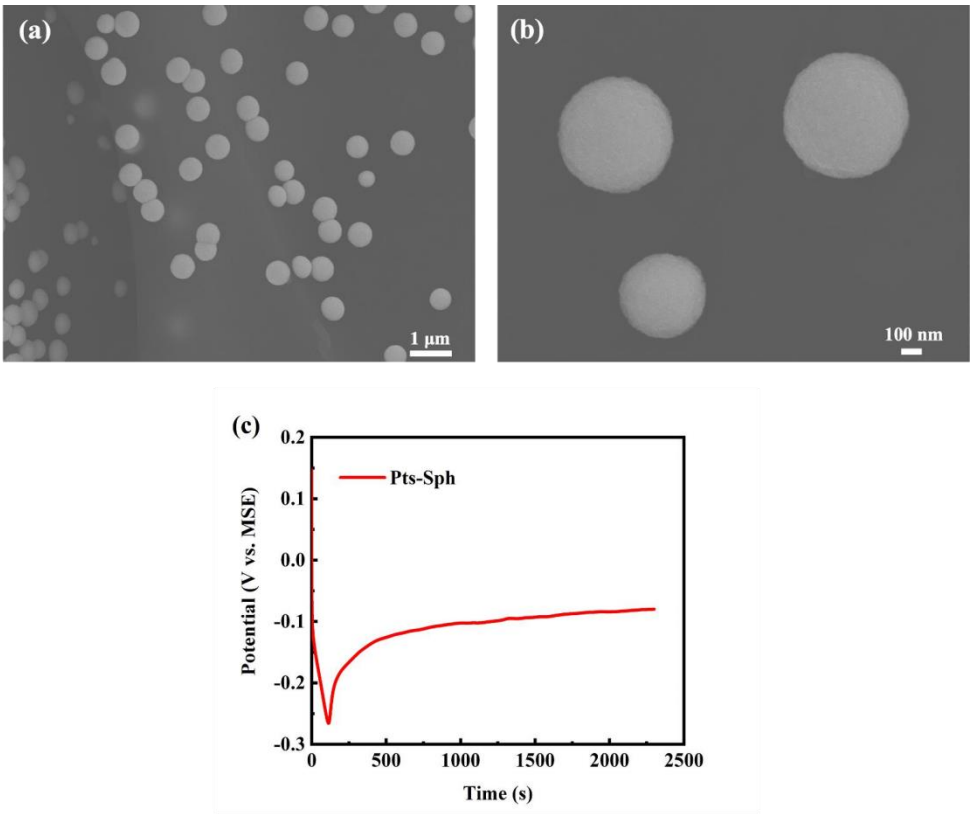

Figure 2. (a) SEM image of the morphology of spherical Pt particles electrodeposited at a current density of –0.4 mA cm^{-2} for 2300 s in a mixed solution of 5 mM H_2PtCl_6 and 0.5 M H_2SO_4, and (b) corresponding high-magnification SEM image (Pts–Sph). (c) Chronoamperograms measured during electrochemical deposition at −0.4 mA cm^{-2} for 2300 s.

In PSWP treatment, the technique parameters, including the E_U, E_L, t, and f, directly determine the electrochemical environment encountered by Pt particles and the particles' morphology. We carried

out a series of experiments with controlled variables to study the functional mechanisms of these parameters on the morphology evolution of the Pt particles. In all cases, Pt particles were first deposited on a carbon paper substrate as they were in the preparation of Pts–Sph. Then, the electrodeposited Pt particles were subjected to PSWP processing in a 1 M H_2SO_4 solution. As shown in Figure 3, *f* and *t* were controlled to 10 Hz and 35 min, respectively. When the E_U was 0.2 V, the size and morphology of the Pt particles remained almost unchanged regardless of the E_L (Figure 3a–c). When the E_U was increased to 0.6 V, the morphology changed from the initial spherical Pt particles to hollow Pt particles (Figure 3d–f). When the E_U was 1 V, as the E_L decreased, many Pt particles with cube-like structures appeared on the surface of the substrate. Furthermore, the deposited Pt particles had a 3D cubic shape. Moreover, as E_L decreased from –2.4 V to –4.0 V, the number of small Pt particles increased. It was clear that with higher E_U and lower E_L, the effect of PSWP on the morphology modification was more obvious.

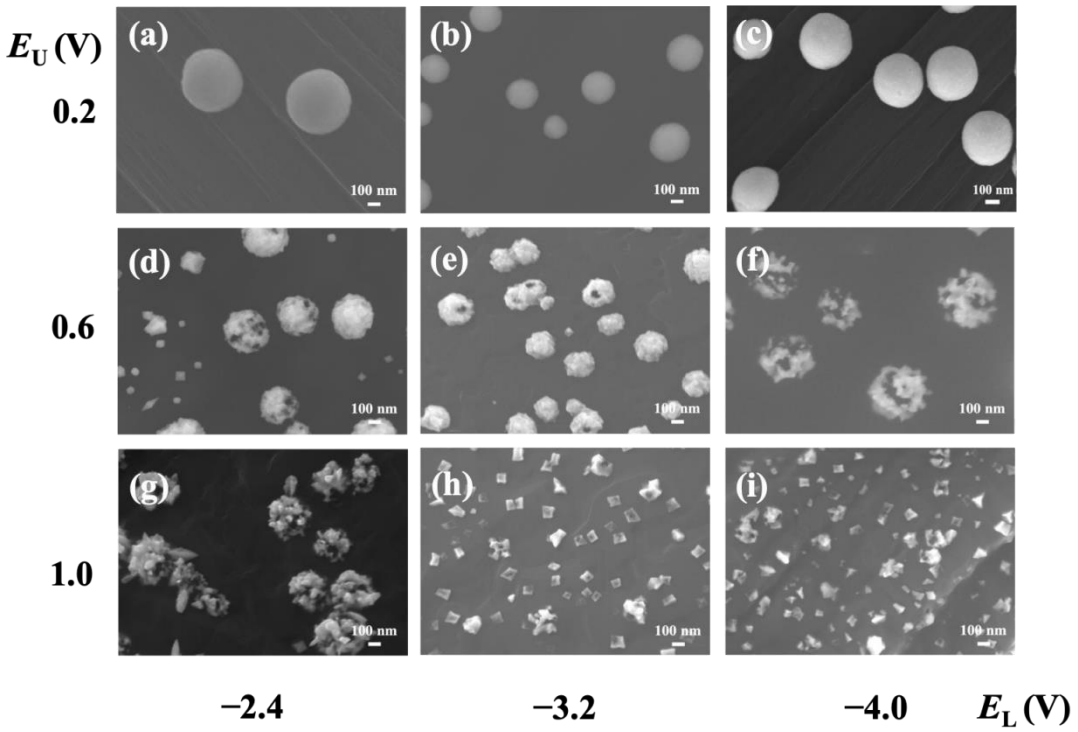

Figure 3. Morphological evolution of Pt particles after the periodic square-wave potential process in 1 M H_2SO_4 solution with (a–i) various E_U and E_L for 35 min at a *f* of 10 Hz.

During the electrochemical modification of Pt particles during the PSWP treatment, only metal-selective electro-dissolution occurred during the anodic half-cycle (E_U process), while in the cathodic half-cycle (E_L process), metal selective electrochemical deposition was the main process. With a low E_U, the Pt particles were hardly oxidized and dissolved as Pt ions into the H_2SO_4 solution during the E_U process. As a result, only hydrogen evolution occurred in the E_L process, and the morphology of Pt particles remained unchanged[22]. As E_U increased, Pt particles were oxidized to Pt ions in the E_U

process, and the dissolved Pt ions were deposited back on the surface of the carbon paper in the E_L process. Since the diffusion of Pt ions occurred throughout the whole modification process, the Pt ions might not have deposited back on the original places from which they dissolved. Therefore, the morphology of Pt particles changed after the PSWP process. Moreover, with a higher E_U, more Pt particles were dissolved throughout the PSWP process, indicating a more significant Pt redistribution. When the E_U reached 1 V, a suitable concentration gradient of Pt ions was formed near the surface of the carbon paper, leading to the deposition of cube-like Pt particles. In addition, with the decrease in E_L, the electrochemical deposition overpotential was higher, leading to an increase in Pt nucleation and the number of small Pt particles.

To study the influence of *t* and *f* during modification on the morphology of Pt particles, E_U (0.9 V) and E_L (–2.7 V) remained unchanged throughout the following PSWP process. Figure 4g–i shows that when *f* was 50 Hz, the morphology and size of Pt particles were almost unchanged compared with those before the PSWP process (Figure 2a and 2b).

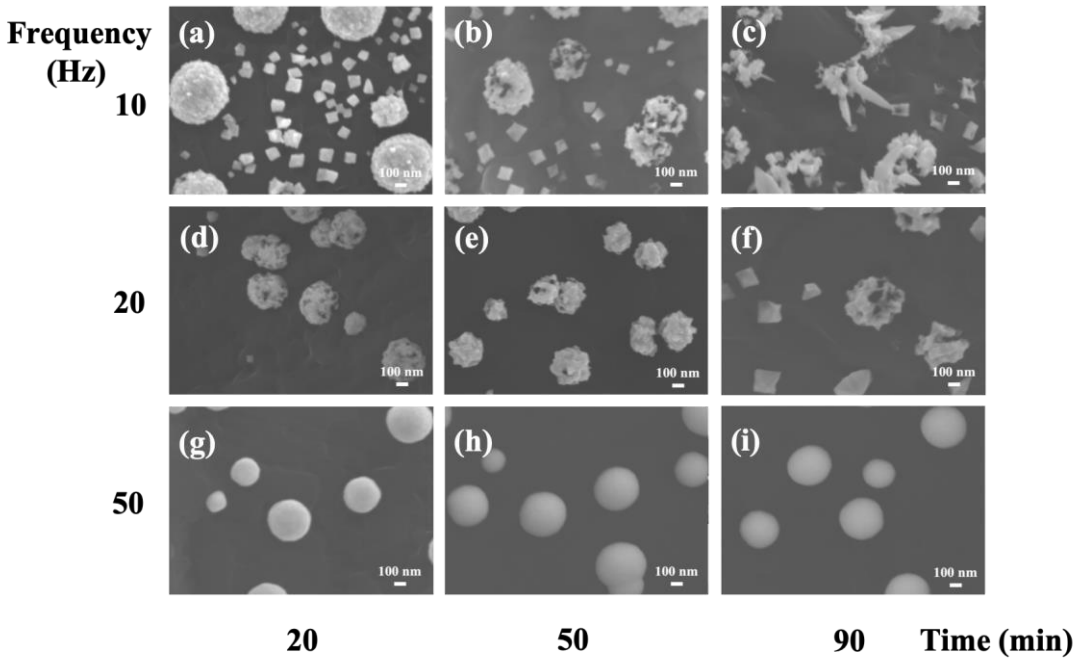

Figure 4. Morphological evolution of Pt particles after the periodic square-wave potential process in 1 M H_2SO_4 solution with (a–i) various *f*; and E_U (0.9 V) and E_L (–2.7 V) remain unchanged.

When *f* dropped to 20 Hz, many pits appeared on the surface of Pt particles, and the size of the particles was slightly reduced to approximately 400 nm (Figure 4d). With the increase in treatment time from 20 min to 90 min, the Pt particles gradually dissolved, and the shape changed from spherical to hollow. As *f* decreased to 10 Hz, some cube-like Pt particles appeared and were present alongside the Pts–Sph (Figure 4a). As *t* increased (90 min), some dendritic Pt particles appeared (Figure 4c). It is shown that a lower *f* and longer *t* brought more morphology changes to Pt particles. In the PSWP process, the value of *f* plays a decisive role because it determines the average thickness of the pulsating diffusion

boundary layer (δ_p), which is related to the migration of soluble Pt species in the solution. The value of δ_p decreases with the reciprocal of $f^{1/2}$[23-25]. The whole process is diffusion controlled[25]. f determines the t of E_U and E_L in a single square wave, and the higher f is, the shorter the single square wave is. When f is high (> 50 Hz), the t of a single E_U process is too short to oxidize Pt particles into Pt ions after the formation of the electric double layer, and thus, the morphology change of the Pt particles is negligible after the PSWP process. In contrast, when f is low (< 10 Hz), a considerable amount of large Pt particles dissolve as Pt ions into the solution during the E_U process, leading to the subsequent electrochemical deposition of small Pt particles and the growth of Pt dendrites during the E_L process.

Figure 5a shows a typical low-magnification transmission electron microscopy (TEM) image of the dendritic Pt particles (Pts–Den, following the same modification as the sample shown in Figure 4c), and the dendrite had a length of 700 nm and a width of 200–300 nm. The edge of the Pt dendrite had a zigzag morphology, which could provide sufficient active sites for the electrocatalytic process. The tip and uneven structure of the Pts–Den and cube-like Pt particles (Pts–Cub, which followed the same modification as the sample shown in Figure 3h) increased the specific surface area of electrocatalysts, which also led to their high electrocatalytic activity[26-28]. High-resolution TEM (HRTEM) showed Pt dendrites with clear lattice fringes.

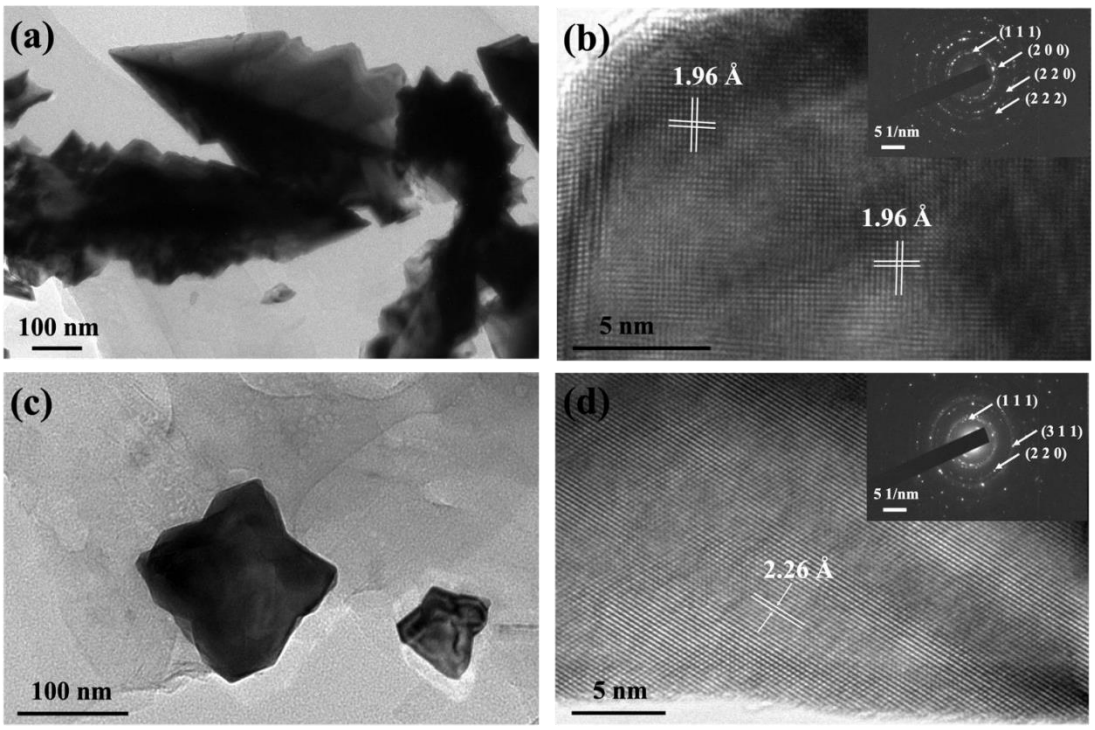

Figure 5. (a) TEM image of Pts–Den and (b) corresponding HRTEM image with the inset showing the corresponding SAED pattern. (c) TEM image of Pts–Cub and (d) corresponding HRTEM image with the inset showing the corresponding SAED pattern.

The interplanar spacing is 1.96 Å, which is entirely consistent with the lattice spacing of the Pt(200) plane[29]. Figure 5b shows the selected area electron diffraction (SAED) pattern corresponding to the HRTEM image, which indicated a typical polycrystalline structure. The SAED patterns for Pts–Den reveal several bright concentric rings (inset in Figure 5b), which were attributed to the Pt(200), Pt(111), Pt(220) and Pt(222) Pt face-centered cubic (fcc) crystal diffractions. Figure 5c shows a TEM image of Pts–Cub, which had an uneven surface that is consistent with that shown in the SEM image (Figure 3h). The corresponding HRTEM image shows a crystal plane spacing of 2.26 Å, which is in good agreement with the Pt(111) plane spacing. The SAED pattern shows a diffraction pattern corresponding to the Pt(111), Pt(220) and Pt(311) lattice planes of fcc Pt from the inset in Figure 5d.

To explore the structure-activity relationship of Pt electrocatalysts, this paper studied the electrocatalytic performance of Pts–Cub, Pts–Den and Pts–Sph in electrochemically-oxidizing methanol and ammonia. A number of studies demonstrated that H adsorption/desorption on Pt in H_2SO_4 solution is highly sensitive to the surface structure of Pt. This experiment can be used to qualitatively characterize the type, density, and preferential orientation of the surface sites of different catalysts, reflecting the electrochemically active surface area (ECSA) of Pt catalysts as shown in Figure 6, cyclic voltammetry (CV) tests of Pts–Den, Pts– Cub, and Pts–Sph particles were performed in 0.5 M H_2SO_4 at a scan rate of 50 mV s^{-1}. Three CVs show typical potential regions, including hydrogen adsorption/desorption (–0.2 V (vs. SCE) to 0.1 V (vs. SCE)), the double-layer potential region (0.1–0.5 V (vs. SCE)), Pt-OH_{ad} (0.5–1.0 V (vs. SCE)) and the formation/reduction of Pt oxide on the surface. Due to the desorption of weakly bonding hydrogen species and strongly bonding hydrogen species, hydrogen desorption peaks formed at –0.15 V (vs. SCE) and –0.05 V (vs. SCE) in the anodic scan, respectively[32]. The H desorption region shows different characteristic peaks due to the different structure/morphology of deposited Pt particles h_1 and h_2. Many studies have reported that the h_1 peak in the CV curve of H_2SO_4 is related to H desorption at Pt(110) sites, and the peaks h_2 is related to Pt(100) step sites and terrace borders[5,30].

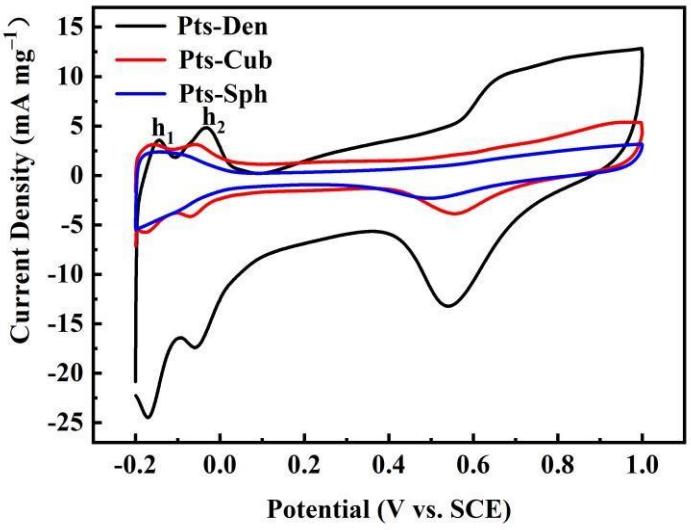

Figure 6. CVs of Pts–Den, Pts–Cub and Pts–Sph in 0.5 M H_2SO_4 solution at 0.05 V s^{-1}.

As shown in Figure 6, compared with the peaks of Pts–Sph Pt particles, Pts–Den shows significant h_1 and h_2 peaks and has a high ratio of h_2/h_1, which confirms the Pt(100) preferential orientation of Pts–Den. The CVs of Pts–Cub also have two noticeable humps, while the low ratio of h_2/h_1 indicates that Pts-Cub does not show the Pt(100) preferred crystal plane. This result is also consistent with the crystal plane structure observed by TEM.

Table 1 shows that the h_2/h_1 of Pts–Den is 1.35. The h_2/h_1 value of Pts–Cub is 1.00, which is higher than the value of 0.70 for spherical particles without electrochemical treatment.

Table 1. The ratio of h_2/h_1 of Pt particles with different morphologies.

No.	h_1 (mA mg^{-1})	h_2 (mA mg^{-1})	h_2/h_1
1 (Pts–Den)	3.57	4.83	1.35
2 (Pts–Cub)	3.13	3.14	1.00
3 (Pts–Sph)	2.37	1.67	0.70

The ECSA (cm^2 cm^{-2}) of the Pt electrocatalyst was derived by calculating the CVs according to the following equation:

$$\mathrm{ECSA}=\frac{Q_{\mathrm{H}}}{Q_{\mathrm{H}}^{0}} \quad (1)$$

The mass-specific, electrochemically active surface area (SSA, cm^2 mg^{-1}) of Pt catalysts can be calculated by:

$$\mathrm{SSA}=\frac{\mathrm{ECSA}}{L_{\mathrm{Pt}}} \quad (2)$$

where Q^0_{H} is the specific charge for a hydrogen monolayer on Pt (0.21 mC cm^{-2})[33], Q_{H} is the charge for hydrogen desorption (mC cm^{-2}) and L_{Pt} is the amount of Pt loading (mg cm^{-2}). The Q_{H} value of the electrocatalyst can be calculated by integrating the area covered by the hydrogen adsorption current peak and subtracting the contribution of the double charge layer. The ECSA of the three samples is shown in Table 2, which will be discussed later.

To investigate the electrocatalytic activity of the Pt particles after PSWP treatment for methanol oxidation, cyclic voltammograms (CVs) of the Pt electrocatalyst were obtained in 0.5 M H_2SO_4 solution containing 1 M CH_3OH at a scan rate of 50 mV s^{-1} (Figure 7), and the current was normalized by Pt loading. It can be seen from the methanol CV curves that the characteristic oxidation peak of methanol in the forward scan appears during the hydrogenation reaction stage of methanol, and the characteristic oxidation peak in the reverse scan represents the removal of adsorbed intermediate carbonaceous species that were formed in the forward scan[34]. The corresponding oxidation peaks of Pts–Den in the forward and reverse scans appeared at about 0.65 V (vs. SCE) and 0.5 V (vs. SCE), respectively. When the potential is at the initial stage of forwarding scanning, methanol molecules were adsorbed on the surface of Pt by the formation of Pt-CO_{ads}. Oxidation of H_2O simultaneously led to the formation of Pt-OH_{ads}[35]. The adsorption of CO_{ads} and oxidation of water increased gradually with a further increase in the current until reaching its maximum value at ~0.65 V (vs. SCE). The current decreased again after the peak formed due to the inhibition of methanol oxidation by the reaction products as the potential increased. The current continued to increase during the oxidation of methanol during the reverse scanning process. The peak observed in the backward scanning process is due to the desorption of CO produced during methanol oxidation[35]. The peak of the current density of Pts–Den when electrocatalysis of methanol reached 280 mA mg^{-1}, which is more than twice that of Pts– Cub and more than five times that of the Pts–Sph Pt particles. Obviously, the Pt particles modified by the PSWP show higher electrocatalytic activity when electrochemically catalyzing methanol (Table 3).

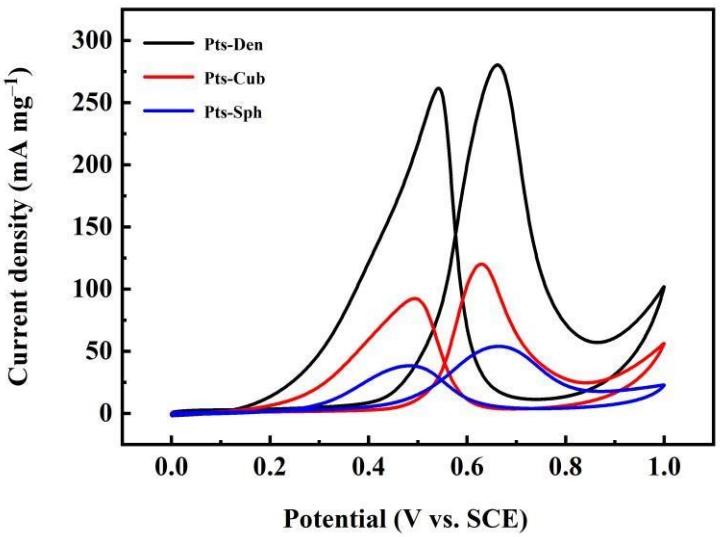

Figure 7. CVs of Pts–Den, Pts–Cub and Pts–Sph in 0.5 M H_2SO_4 and 1 M CH_3OH solution at a scan rate of 0.05 V s^{-1}.

Figure 8 shows the CVs of Pts–Den, Pts–Cub and Pts–Sph in 1 M KOH and 0.1 M NH_3 solutions. The current was normalized by Pt loading. The CVs show a well-defined anodic current peak at –0.24 V (vs. SCE), which is due to the electrochemical oxidation of ammonia to produce N_2[36,37]. The current density of Pts–Den for electrochemical oxidation of ammonia is more than twice that for the

other two electrocatalysts, and showed higher catalytic performance (Table 3). The MA of Pts–Den was more than twice than that of Pts–Cub and more than five times than that of the Pts–Sph Pt particles during the electrooxidation of methanol (Table 2). In addition, the MA of Pts–Den is more than 2 times than that of two other electrocatalysts in ammonia oxidation (Table 2).

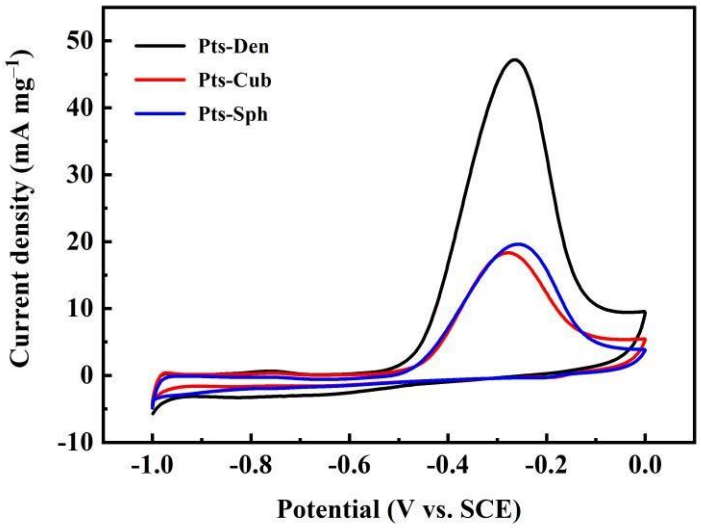

Figure 8. CVs measured on Pts–Den, Pts–Cub and Pts–Sph in 1 M KOH and 0.1 M ammonia solution at a scan rate of 0.01 V s^{-1}.

Generally, the mass-specific activity (MA) of an electrocatalyst can be simply expressed as[38]:

$$MA = SSA \times SA \quad (3)$$

SA is the specific activity, which is defined as the current normalized by the electrochemically active surface area. The SA was calculated based on the electrochemically active surface area (Figure 6) and the current density (Figure 7, Figure 8).

Table 2. Calculated ECSA, L_{Pt}, SA and MA of different Pt electrocatalysts for the electrooxidation of methanol and ammonia.

Samples No.			Methanol oxidation		Ammonia oxidation	
	ECSA, $cm^2\ cm^{-2}$	L_{Pt}, mg	SA, $mA\ cm^{-2}$	MA, $mA\ mg^{-1}$	SA, $mA\ cm^{-2}$	MA, $mA\ mg^{-1}$
1 (Pts–Den)	4.00	0.07	4.91	280	0.82	47
2 (Pts–Cub)	5.33	0.14	3.16	120	0.53	18
3 (Pts–Sph)	6.10	0.22	1.93	54	0.64	20

Table 3. The electrocatalyst prepared in this work was compared with the performance of other catalysts for methanol and ammonia electrooxidation described in previous work.

Catalyst type	Preparation method	Test protocol	Mass activity (mA mg^{-1})	Reference
Methanol electrooxidation				
Dendritic Pt particles (this work)	Pt modified by periodic square wave	CV in 0.5 M H_2SO_4 + 1 M CH_3OH at 0.05 V s^{-1}	280	–
Pt nanoparticles loaded on carbon foams	Ethylene glycol reduction method	CV in 0.5 M H_2SO_4 + 1 M CH_3OH at 0.05 V s^{-1}	146.6	[39]
Pt hollow cubes	Ethylene glycol reduction method	CV in 0.5 M H_2SO_4 + 0.5 M CH_3OH	242	[40]
Flower-like Pt particles	Potentiostatic electrochemical deposition	CV in 0.5 M H_2SO_4 + 0.5 M CH_3OH at 0.05 V s^{-1}	87.7	[41]
Pt on flower-like SnO_2	Hydrothermal method	CV in 0.5 M H_2SO_4 + 1 M CH_3OH at 0.05 V s^{-1}	211.2	[42]
Ammonia electrooxidation				
Dendritic Pt particles (this work)	Pt modified by periodic square wave	CV in 1 M KOH + 0.1 M NH_3 at 0.01 V s^{-1}	47	–
Amorphous, boulder-like Pt deposits	Galvanostatic electrochemical deposition	CV in 1 M KOH + 1 M NH_3 at 0.01 V s^{-1}	~22	[43]
Flower-like Pt particles	Potentiostatic electrochemical deposition	CV in 1 M KOH + 0.1 M NH_3 at 0.01 V s^{-1}	30	[44]
Sheet-like Pt particles	electrochemical deposition by CV	CV in 1 M KOH + 0.1 M NH_3 at 0.05 V s^{-1}	~45.9	[45]
Well-dispersed Pt nanosheets	Potentiostatic electrochemical deposition	CV in 1 M KOH + 0.1 M NH_3 at 0.01 V s^{-1}	70	[44]
Layered Pt-Rh on carbon fibers	Galvanostatic electrochemical deposition	CV in 0.1 M KOH + 1.03 mM NH_4OH at 0.0033 V s^{-1}	~5.8	[46]

The superb electrocatalytic performance of Pts–Den is due to its (100) preferential crystal planes that appeared after the PSWP process, since the electrocatalytic oxidation of ammonia is sensitive to the (100) crystal plane of Pt[30,47]. In addition, the zigzag edges formed during the PSWP treatment also

provide sufficient active sites for electrocatalysis. This illustrates the feasibility of PSWP in improving electrocatalyst performance and provides a new method for preparing high-performance electrocatalysts.

4. CONCLUSIONS

In this work, we first obtained spherical Pt particles (Pts–Sph) by constant current electrochemical deposition. Then, the spherical Pt particles were subjected to PSWP treatment to prepare dendritic Pt particles (Pts–Den) and cubic Pt particles (Pts–Cub). The obtained electrocatalyst was used for the electrochemical oxidation of methanol and ammonia. We explored the evolution of the electrocatalyst morphology under the four PSWP parameters (E_U and E_L, f and t). It was found that a lower f and longer t would lead to more morphological changes of the Pt particles. Pt electrocatalysts could dissolve and deposit faster when subjected to higher E_U and lower E_L. Through the proper combination of f, t, E_U, and E_L, the morphology and size of the electrocatalyst obtained by constant current electrochemical deposition were changed, and electrocatalysts with different morphologies could be prepared. HRTEM and SAED showed that the Pts–Den and Pts–Cub electrocatalysts were both polycrystalline, and the Pts–Den presented preferential (100) crystal faces. Then, the Pts–Den and Pts–Cub were used to electrocatalyze methanol and ammonia. When the Pts–Den electrocatalyzed methanol and ammonia, the MA values were approximately 5 times and 2 times than that of Pts–Sph. This work proposed a promising method to prepare Pt electrocatalysts with high electrocatalytic activity by changing their morphology and structure.

ACKNOWLEDGEMENTS
This work was supported by the National Natural Science Foundation of China (Nos. 51771134, 51801134), Tianjin Natural Science Foundation for Distinguished Young Scholar (No. 18JCJQJC46500), Tianjin Natural Science Foundation (No. 20JCQNJC01130), National Natural Science Foundation of China and Guangdong Province (No. U1601216), and the National Youth Talent Support Program.

References

1. T. Radhakrishnan and N. Sandhyarani, *Int. J. Hydrogen Energy*, 42 (2017) 7014–7022.
2. X. Zhang and L. X. Ma, *J. Power Sources*, 286 (2015) 400–405.
3. K. Hara, M. Kamata, N. Sonoyama and T. Sakata, *J. Electroanal. Chem.*, 451 (1998) 181–186.
4. J. Liu, B. Chen, Z. Ni, Y. Deng, X. Han, W. Hu and C. Zhong, *ChemElectroChem*, 3 (2016) 537–551.
5. A. Ponrouch, S. Garbarino, E. Bertin, C. Andrei, G. A. Botton and D. Guay, *Adv. Funct. Mater.*, 22 (2012) 4172–4181.
6. Y. Bing, H. Liu, L. Zhang, D. Ghosh and J. Zhang, *Chem. Soc. Rev.*, 39 (2010) 2184–202.
7. F. J. Vidal-Iglesias, J. Solla-Gullón, V. Montiel, J. M. Feliu and A. Aldaz, *J. Power Sources*, 171 (2007) 448–456.
8. J. Xu, S. Wang, Z. Du, J. Zhu, Y. Liu, W. Zhang and J. Wang, *Micro Nano Lett.*, 8 (2013) 890–894.
9. H. Y. Chou, T. K. Yeh and C. H. Tsai, *Int. J. Electrochem. Sci.*, 9 (2014) 5763–5775.

10. C. Zhong, W. B. Hu and Y. F. Cheng, *J. Mater. Chem. A*, 1 (2013) 3216–3238.
11. A. Kabbabi, F. Gloaguen, F. Andolfatto and R. Durand, *J. Electroanal. Chem.*, 373 (1994) 251–254.
12. S. Mukerjee, *J. Appl. Electrochem.*, 20 (1990) 537–548.
13. J. Ding, Z. Liu, X. R. Liu, J. Liu, Y. D. Deng, X. P. Han, C. Zhong and W. B. Hu, *Adv. Energy Mater.*, 9 (2019) 1900955.
14. J. M. Kim, H. Joh, S. M. Jo, D. J. Ahn, H. Y. Ha, S. Hong and S.-K. Kim, *Electrochim. Acta*, 55 (2010) 4827–4835.
15. T. S.Ahmadi, Z. L. Wang, T. C. Green, A. Henglein and M. A. El, *Science*, 272 (1996) 1924–1926.
16. W. Yang, Y. Wang, J. Li and X. Yang, *Energy Environ. Sci.*, 3 (2010) 144–149.
17. J. Ding, Z Liu, X. R. Liu, B. Liu, J. Liu, Y. D. Deng, X. P. Han, W. B. Hu and C. Zhong, *Angew. Chem. Int. Ed.*, 59 (2020) 5092–5101.
18. S. Li, H. Chen, J. Liu, Y. Deng, X. Han, W. Hu and C. Zhong, *ACS Appl. Mater. Interfaces*, 9 (2017) 27765–27772.
19. C. F. Zinola, *Electrochem. Commun.*, 87 (2018) 35–39.
20. J. Liu, C. Zhong, Y. Yang, Y. T. Wu, A. K. Jiang, Y. D. Deng, Z. Zhang and W. B. Hu, *Int. J. Hydrogen Energy*, 37 (2012) 8981–8987.
21. F. Ye, C. Xu, G. Liu, M. Yuan, Z. Wang, X. Du and J. K. Lee, *Energy Convers. Manage.*, 160 (2018) 85–92.
22. J. L. Zubimendi, G. Andreasen and W. E. Triaca, *Electrochim. Acta*, 40 (1995) 1305–1314.
23. A. R. Dedpic and K. I. Popov, *J. Appl. Electrochem.*, 1 (1971) 275–278.
24. N. Ibl, *Surf. Technol.*, 10 (1980) 81–104.
25. J. Zubimendi, G. Andreasen and W. Triaca, *Electrochim. Acta*, 40 (1995) 1305–1314.
26. A. Siriviriyanun and T. Imae, *Phys. Chem. Chem. Phys.*, 15 (2013) 4921–4929.
27. Z. Li, S. Ji, B. G. Pollet and P. K. Shen, *J. Nanopart. Res.*, 15 (2013) 1959.
28. J. Liu, X. Fan, X. Liu, Z. Song, Y. Deng, X. Han, W. Hu and C. Zhong, *ACS Appl. Mater. Interfaces*, 9 (2017) 18856–18864.
29. J. Liu, X. Du, Y. Yang, Y. Deng, W. Hu and C. Zhong, *Electrochem. Commun.*, 58 (2015) 6–10.
30. E. Bertin, S. Garbarino, D. Guay, J. Solla-Gullón, F. J. Vidal-Iglesias and J. M. Feliu, *J. Power Sources*, 225 (2013) 323–329.
31. R. A. Martinez-Rodriguez, F. J. Vidal-Iglesias, J. Solla-Gullon, C. R. Cabrera and J. M. Feliu, *J. Am. Chem. Soc.*, 136 (2014) 1280–1283.
32. N. M. Markovic and P. N. Ross Jr, *Surf. Sci. Rep.*, 45 (2002) 117–229.
33. E. Antolini, L. Giorgi, A. Pozio and E. Passalacqua, *J. Power Sources*, 77 (1999) 136–142.
34. H. Zhao, C. Yu, H. You, S. Yang, Y. Guo, B. Ding and X. Song, *J. Mater. Chem.,* 22 (2012) 4780–4789.
35. H. M. Ghartavol, R. S. Moakhar and A. Dolati, *J. Chem. Sci.*, 129 (2017) 1399–1410.
36. S. Le Vot, L. Roué and D. Bélanger, *J. Electroanal. Chem.*, 691 (2013) 18–27.
37. K. Endo, K. Nakamura, Y. Katayama and T. Miura, *Electrochim. Acta*, 49 (2004) 2503–2509.
38. E. Antolini and J. Perez, *J. Mater. Sci.*, 46 (2011) 4435–4457.
39. X. J. Bian, K. Qian, L. Liao, X. F. Zhou, K. Guo, X. D. Huang, C. Z. Yu, C. Ji and B. H. Liu, *ECS Electrochem. Lett*., 3 (2014) F11–F14.
40. C. Li, B. Jiang, M. Imura, V. Malgras and Y. Yamauchi, *Chem. Commun*., 50 (2014) 15337–15340.
41. R. Ojani, E. Hasheminejad and J. B. Raoof, *Energy*, 90 (2015) 1122–1132.
42. H. Zhang, C. Hu, X. He, L. Hong, G. Du and Y. Zhang, *J. Power Sources*, 196 (2011) 4499–4505.
43. M. Cooper and G. Botte, *J. Electrochem. Soc*. 153 (2006) 1894–1901.
44. X. T. Du, Y. Yang, J. Liu, B. Liu, J. B. Liu, C. Zhong and W. B. Hu, *Electrochim. Acta*, 111 (2013) 562–566.
45. J. Liu, W. Hu, C. Zhong and Y. F. Cheng, *J. Power Sources*, 233 (2013) 165–174.

46. P. Bonnin, J. Biddinger and G. Botte, *J. Power Sources*, 182 (2008) 284–290.
47. C. Zhong, J. Liu, Z. Y. Ni, Y. D. Deng, B. Chen and W. B. Hu, *Sci. China Mater*. 57 (2014) 13–25.